Research Article Open Access

David C. Cox*, John C. Gallop, Ling Hao

Focused Ion Beam Processing of Superconducting Junctions and SQUID Based Devices

Abstract: Focused ion beam (FIB) has found a steady and growing use as a tool for fabrication, particularly in the length-scale of micrometres down to nanometres. Traditionally more commonly used for materials characterisation, FIB is continually finding new research areas in a growing number of laboratories. For example, over the last ten years the number of FIB instruments in the U.K. alone has gone from single figures, largely supplied by a single manufacturer, to many tens of instruments supplied by several competing manufacturers. Although the smaller of the two research areas, FIB fabrication has found itself to be incredibly powerful in the modification and fabrication of devices for all kinds of experimentation. Here we report our use of FIB in the production of Superconducting QUantum Interference Devices (SQUIDs) and other closely related devices for metrological applications. This is an area ideally suited to FIB fabrication as the required precision is very high, the number of required devices is relatively low, but the flexibility of using FIB means that a large range of small-batch, and often unique, devices can be constructed quickly and with very short lead times.

Keywords: Focused Ion Beam, SQUID, Nanofabrication

Doi: 10.2478/nanofab-2014-0005
received March 20, 2014; accepted May 13, 2014

1 Introduction

SQUIDs are typically macroscopically large objects operating in the quantum regime and are capable of measuring a wide range of physical parameters [1-4]. The unequalled sensitivity due to quantum interference effects with matter offers a diverse range of uses that very few if any other devices can compete with. The natural and most straightforward quantity that a SQUID responds to directly is magnetic flux, although other quantities as diverse as spatial displacement, photon detection, or even mass detection, when combined with a mechanical resonator, are possible [3, 5–7]. The first SQUID devices developed were of relatively large size (typically tens of micrometres or often more in linear dimension) [8]. It has only recently been appreciated that SQUID size may be radically reduced towards the nanoscale and that such devices will not only retain exceptional sensitivity but will, through their size, find applications in a whole new range of detection and measurement areas [9–13]. An example of performance gain by reduction of the SQUID size is given in equation 1, where the minimum detectable energy change a SQUID can measure, is described.

$$\varepsilon_n = \frac{\langle S_\varphi^2 \rangle}{2L} = 16 k_B T (LC)^{1/2} \quad (1)$$

Here ε_n, is the minimum detectable energy change where S_ϕ, is the spectral noise density and L and C the inductance and capacitance of the SQUID loop, the temperature is given by T and k_B is the Boltzmann constant. Clearly an improvement in the energy sensitivity can be attained by a reduction in the operating temperature. Alternately, we can effect similar improvement by reducing the inductance and capacitance of the SQUID loop by reducing its size. The FIB allows us to easily reduce loop dimensions down to submicron, without the need for more complex electron beam lithography.

Restrictions on operating ever-smaller SQUIDs have arisen for several reasons. First, "traditional" SQUIDs, incorporating Josephson tunnel junctions, are generally found to have dimensions greater than 1 μm, due to junction current-density limitations. They also require a trilayer deposition route, which requires an oxidation treatment. Second, tunnel junctions also possess significant capacitance, arising from their geometry. It has been recognized that the use of microbridge junctions would very effectively reduce the junction

*Corresponding author: David C. Cox : Advanced Technology Institute, University of Surrey, Guildford, Surrey, GU2 7XH, U.K., david.cox@npl.co.uk
David C. Cox, John C. Gallop, Ling Hao: National Physical Laboratory, Hampton Road, Teddington, Middlesex, TW11 0LW, U.K.

size and capacitance, thereby allowing smaller SQUID inductance. In this paper we describe the production of nanobridge junctions, qualitatively describe the influence of gallium (Ga) ion milling (and the inevitable associated implantation) on the niobium (Nb) films as they are patterned into micro/nanobridge junctions in this way. We then turn our attention to focus on our simple fabrication method for making superconducting nanoscale Josephson devices which we then extend to producing nanoscale SQUIDs, based on focused ion beam (FIB) fabrication [14]. We will show the exceptional measurement sensitivity and low noise performance which has long been known from macroscopic devices extends down, unabated, to the nanoscale. The devices fabricated by this FIB method have shown excellent performance [15] but it should be stated that some basic properties of the Josephson junctions are neither fully characterised or completely understood. We have described our investigations of the basic properties of the SQUID loops including cryogenic resistance versus temperature ($R(T)$) and current– voltage characteristic (IVC) measurements. We finally show examples of the use of FIB fabricated SQUID loops in a series of experiments including nanomagnetism, nanomechanical motion and dosimetry.

2 Nb/Ga-ion interactions

As is well known the interaction of high-energy ions with a solid substrate at normal incidence results in implantation of the ion species and sputtering of the target material with very few ion recoils occurring. In a focused ion beam instrument the ion species used is most likely to be gallium, although noble gas sources and ions from alloy-based sources such as gold silicide are also used. In the case of Ga the typical beam energy will be in the keV range and most likely 30 keV, where the optics of ion columns are optimised to produce the smallest beam spots by most manufacturers of these instruments.

In very general terms the implant depth of the ions and the sputter yield (atoms/ion) scales with mass of the target species. However, whereas implant depth follows this general rule fairly well, for sputter yield this is not a simple linear relationship and some species will deviate significantly from this trend. For example for a 30 keV Ga ion at normal incidence Si has a sputter yield of around 2.6 A/I (mean implant depth ~27 nm), Ag has A/I of 20 (implant depth of ~10 nm), Au has 22 (implant depth ~7.5 nm) but W only 2.5 A/I (implant depth ~7.4 nm). Furthermore, in many cases target materials are not elementally pure but are compounds, or alloys, adding considerable complexity to predicting sputter yields and implant depths. Fortunately, in our case one of the key materials for producing SQUIDs is the type II metallic superconductor niobium, having a superconducting transition at 9.25 K. Irradiating Niobium with a Ga FIB at 30 keV results in ion sputter yields of almost 4 A/I with mean implant depths in the range of 11.5-12.5 nm [16,17] and a maximum possible implant depth approaching 40 nm (Figure 1).

However, discussion of implant depth and sputter yield is incomplete without consideration of the actual ion dose. For example, at high beam currents in excess of 1 nA, if the beam spot is stepped in increments much smaller than the beam spot itself (i.e. with a large beam overlap) and high dwell time, the local ion dose, and therefore number of sputtered atoms is so high that a thin metal film can be completely removed in a matter of seconds. Figure 2: shows a plot of ion dose in ions/μm^2/ms for a range of ion beam currents and beam step sizes (for simplicity the x and y beam steps are set to be equal in this case, and is actually common practice for most FIB applications). We have only plotted beam currents up to 1 nA and x and y steps up to 100 nm. Marked on the plot are the typical conditions where we would be milling a Nb film to make a SQUID device, corresponding to an ion dose of 6 x 10^6 ions/μm^2/ms (50 pA beam current, 7 nm x and y beam step, 1 ms beam dwell time). For comparison a monolayer of Nb metal will have approximately 9 x 10^6 atoms in 1 μm^2. Here we made some simplifications to ignore crystallography of the metal and possible crystal orientations and have worked on the basis of number of atoms in 1 μm^3 of Nb at room temperature and pressure.

Using this simple calculation of atom density and knowing our ion dose we can make some predictions of the expected ion milling rate for an Nb thin film. Here our simple assumptions work quite well as we can neglect redeposition due to milling a thin film only, and although we do see some preferential milling of particular crystal orientations in the film (Figure 3) as milling progresses we still completely remove the film in the predicted time.

Figure 4, shows a plot of expected sputtering rates for given ion doses in the Nb thin film along with predictions of the damage generated. At our regular milling dose of 6 x 10^6 ion/mm^2/ms this results in the sputtering of 2.7 monolayers of Nb per repeat of the pattern corresponding to approximately 1 nm. Allowing for the protective tungsten layer, discussed later on, we can reasonably predict how many repeats of the pattern are required to remove our film and we have found this very simple approach to be quite robust for Nb thin films with slightly more than 200 passes of the beam removing 200 nm of film.

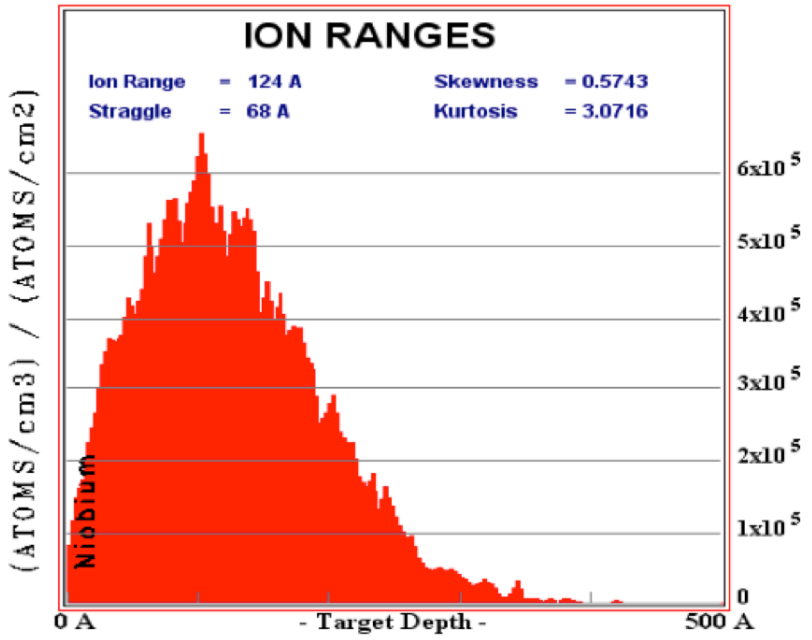

Figure 1: Ga ion implant range in Nb calculated using SRIM (10^4 ion collisions simulated).

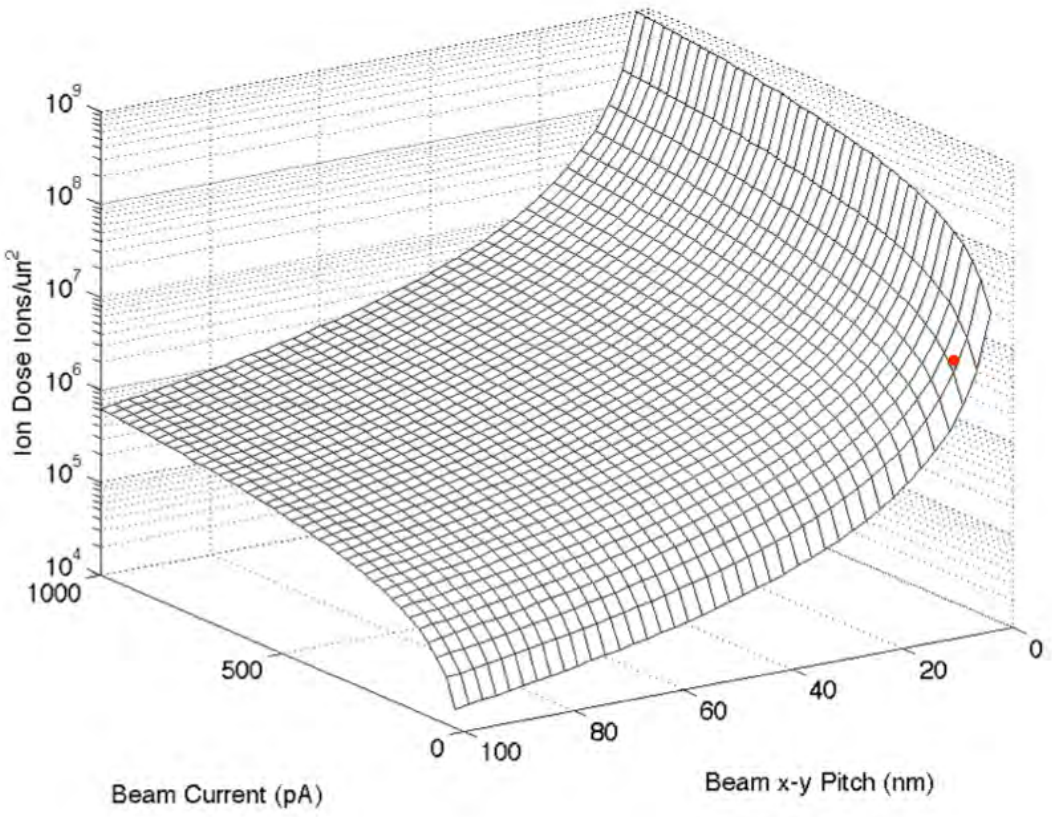

Figure 2: Ion dose in ions/μm^2/ms for given beam conditions. Red dot indicates our typical milling conditions for a Nb thin film.

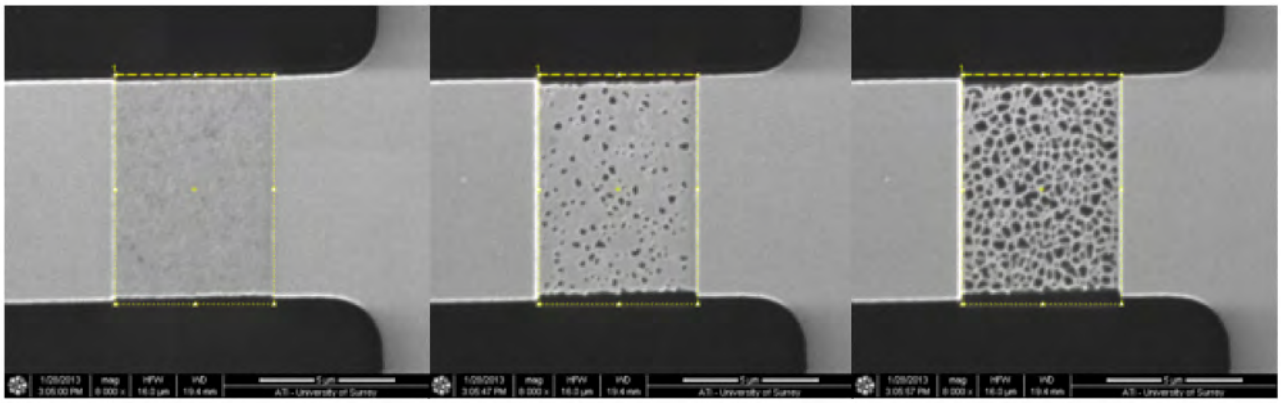

Figure 3: Ion beam images of the evolution of milling in a region of Nb thin film. Preferential milling occurs in certain grains of the film, but over time the film is completely removed with minimal unevenness in the underlying SiO_2 substrate.

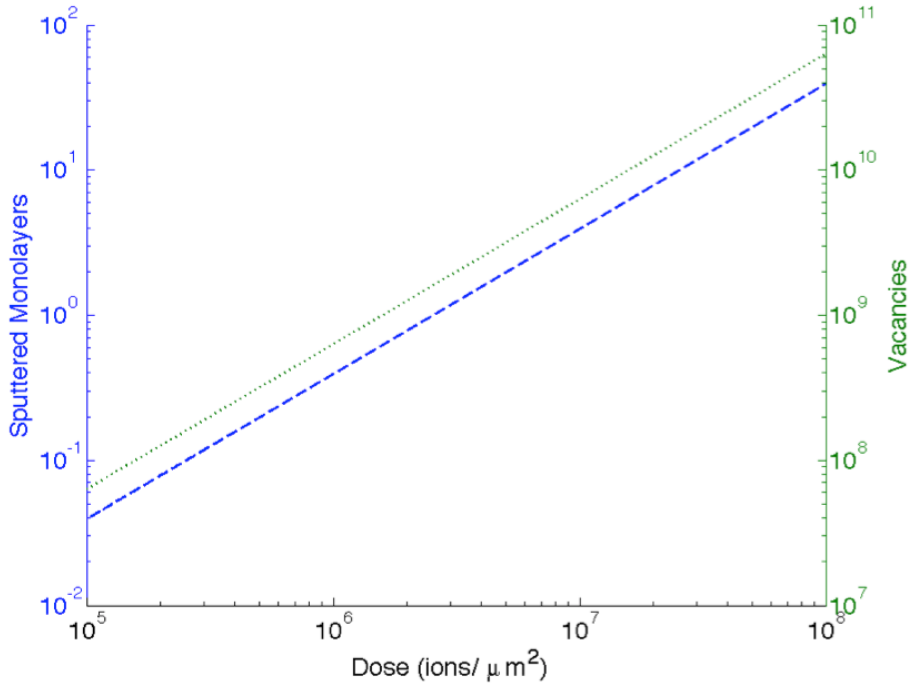

Figure 4: Plot of sputtering rate (left y-axis in blue) and damage accumulation (right y-axis in green) for a given ion dose in a Nb thin film.

Also shown in Figure 4 is a SRIM prediction of the damage induced by the ion beam at given doses. As can be seen at our expected ion dose SRIM predicts well in excess of 10^9 vacancies generated in the implanted volume. Vacancy generation this high would result in complete amorphisation of the Nb lattice in this region, but in practice it would be expected that many vacancies would heal during further ion collisions and Nb atom displacements. However, this region of the film would still be very disrupted and of course implanted with significant Ga. It would be expected that this damage and implantation leads to significant changes in the superconducting properties of the Nb in this region. In fact it appears that all superconductivity is lost if the ion dose is high enough, but the superconducting transition temperature can be modified by the application of careful ion doses. This is discussed in the section on device performance. The complete loss of superconductivity in high ion dose Nb films can however still be exploited to our advantage and is in fact one of the key aspects of how and why our devices are viable. Figure 5 shows schematically the process of producing our superconducting junctions.

The device structure for our superconducting junctions shown schematically in Figure 5a) is based on a p-type 001 Si wafer with 100-200 nm of SiO_2 grown on the top-side. Deposited on this is a Nb film usually

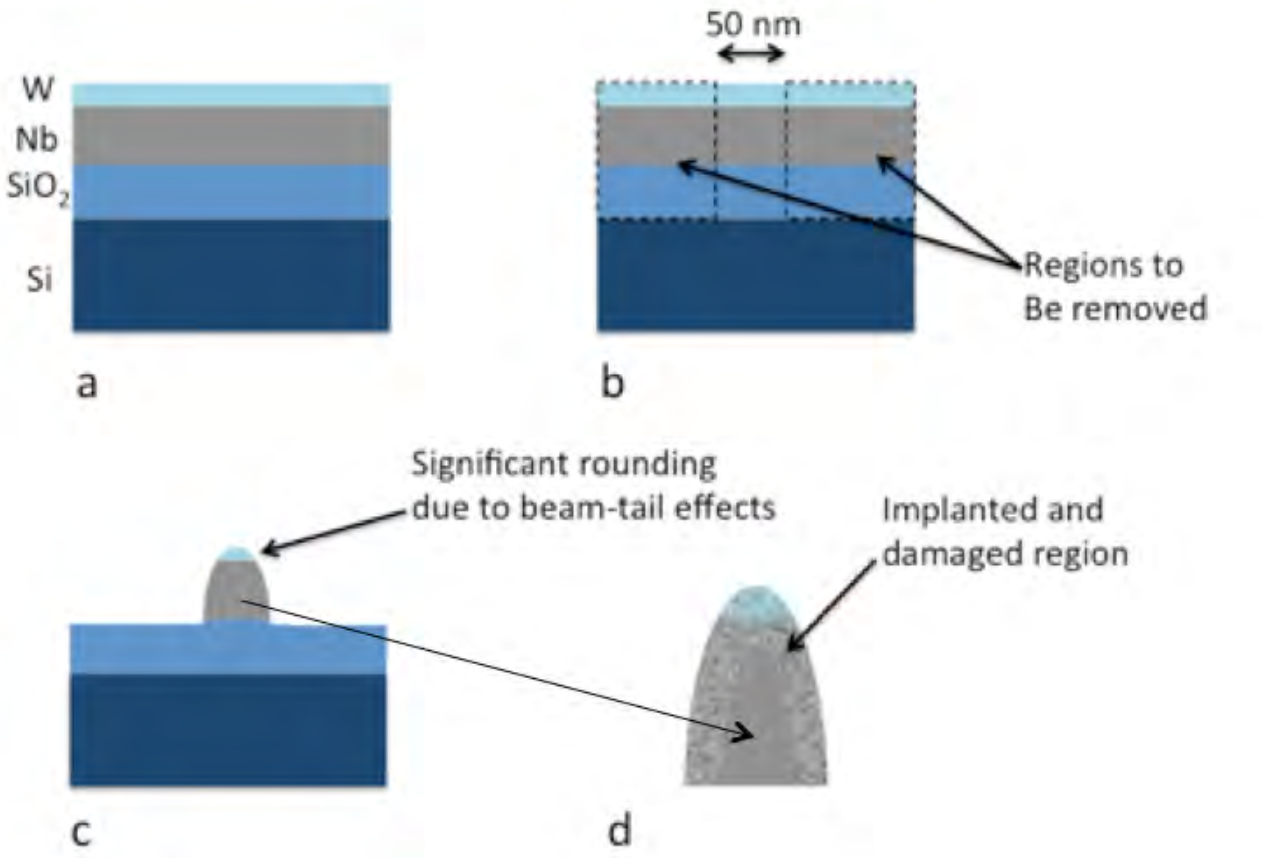

Figure 5: Schematic diagrams of the milling of weak-link superconducting junctions in Nb (not to scale). a) layout of the film. b) Regions to be removed by FIB. c) Actual finished junction geometry. d) Close-up view of implanted and damaged region of finished junction.

200 nm thick by electron beam evaporation in ultra-high-vacuum. Not shown is a 5 nm Cr adhesion layer deposited prior to the Nb to assist with the bonding of the Nb to the SiO_2. On top of the Nb is a thin film (50 nm) of electron beam deposited tungsten hexacarbonyl put down by the electron beam in the FIB to protect the film from ion beam exposure when aligning to the region to be milled. Usually this is only deposited in the region we intend to create a SQUID loop or junction and is no more than a pad of 10 µm x 10 µm. To create the junctions a milling pattern is created that removes material from either side of the junction region (Figure 5b). Here we aim to produce a thin track of material that is 50 nm wide that will form the superconducting junction. However, as is commonly known with FIB the beam spot is not the idealised cone focusing into tight spot of fixed diameter but a larger spot with a Gaussian profile where the quoted spot size is actually the full width half maximum (FWHM) of the Gaussian. What this means in practice is that when milling two adjacent regions with very small separation the beam tails overlap leading to some milling in the area between these regions, in-turn leading to a rounding of the top of the remaining material (Figure 5c).

Turning now to Figure 5d showing the presence of an implanted and damaged zone in the outer regions of the milled junction. When we study the film and junctions regions electrically we see the presence of several distinct features. There are two superconducting transitions, the first occurring at a higher temperature is consistent with the non-milled film, but a second reduced *Tc* is also present and is consistent with the presence of a weak-link junction of reduced cross-section. This is the basic superconducting junction that we produce. It should be noted that these are not classical Josephson junctions of superconductor/insulator/superconductor or superconductor/normal-metal/superconductor (see [1] for descriptions of classical junctions).

The other significant electrical feature we see with junctions of this type is the presence of a parallel shunt-resistor that is of vital importance to the operation of our devices. When the superconductivity of the junction is broken either by the high-temperature, high-current or the presence of high external field, junctions that are on the nanoscale have great difficulty in carrying the electrical current and surviving the subsequent joule heating. The shunt in our systems can assist in carrying this current

loading when the junction loses its superconductivity, but the shunt is not superconducting and plays no role in normal operation. The very act of milling the Nb film produces a thin skin of damaged and implanted material over the junction and produces the shunt. This is very important as it implies that we do not need to produce the smallest junctions possible for two reasons. Firstly, if we attempt to mill the junction as small as we can we will completely destroy their superconducting behaviour due to the implantation damage and introduction of Ga. Secondly, very small junctions even if they could be made will not have the parallel shunt and be prone to damage when superconductivity breaks down. Allowing for a mean implant depth of 12.5 nm, and slightly smaller lateral straggle, from our SRIM simulations, this would imply that if we observe 50 nm junctions in the SEM they actually contain at most a superconducting core of around 25 nm, (almost certainly much smaller than this) with the remainder acting as the parallel shunt.

3 SQUID device fabrication

Our NanoSQUIDs are fabricated by a combination of conventional optical lithography, metal deposition and additional focused ion beam (FIB) milling steps. We have produced a number of generic device structures, which at their simplest are basic four terminal connected leads and bond pads in superconducting material, and at their more complex, suspended silicon nitride windows with device structures in superconducting material on both upper and lower sides of the window. One thing that is common with all of these structures is that there are no SQUID devices or superconducting junctions patterned in the device during the lithography and metal film deposition stages. An example of one of our films is shown in Figure 6.

Here it can be seen that this device structure consists of a simple patterned niobium metal film. The substrate is SiO_2 covered single-crystal silicon (250 nm SiO_2 on p-type doped 001 oriented wafer) and the Nb film (200 nm thick) incorporating leads and bond pads is deposited by electron beam evaporation in ultra-high vacuum with 3-5 nm Cr adhesion layer. The bond pads for the device, right on the edge of the imaged area in this figure, are usually 250 mm squares. The deposition step being essentially single process is incapable of producing SQUID junctions and these are produced by a direct-write method using FIB, with the ion column controlled *via* a Nanometer Pattern Generation System (NPGS) [18]. The NPGS system is derived from a third-party add-on electron beam lithography system, but in our case is adapted to control the ion column scan coils and beam blanker. The patterning options this system gives us are considerably greater than any currently offered by the FIB instrument manufacturers, with exceptional control of patterning strategy and its implementation.

Figure 7 shows a zoomed in micrograph closer to the device region. This example of one of our film structures has a large loop of 25 μm diameter that can, with suitable FIB modification, be converted into a large SQUID loop, but still with nanoscale weak link junctions. As can also be seen in this figure, there are several regions where the

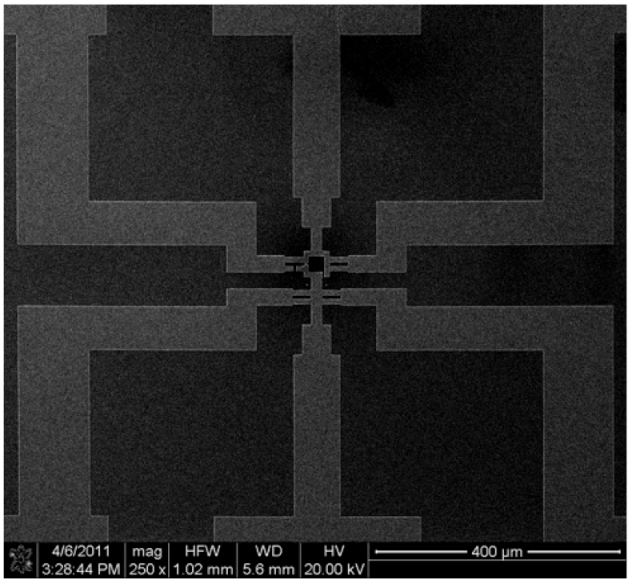

Figure 6: Low magnification SEM image of one of our typical device structures.

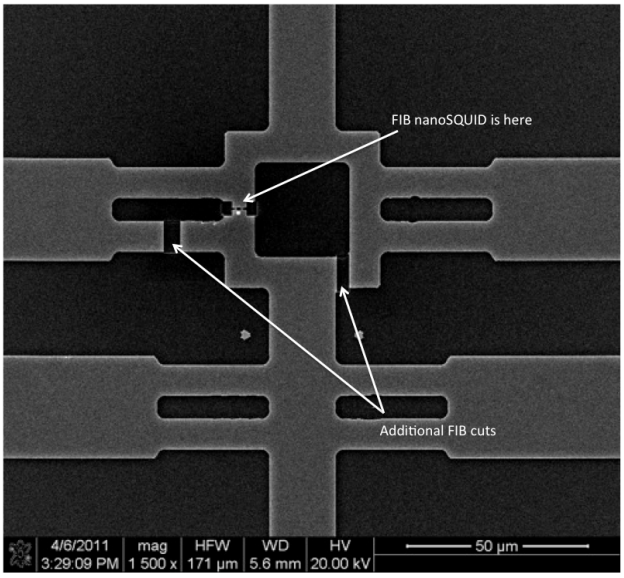

Figure 7: Higher magnification micrograph of one of our device films showing the modifications to the film leads and the location of the nanoSQUID.

film has been cut with FIB so that the conduction path can only be through the nanoSQUID. Our film pattern designs give us great flexibility and we can pattern SQUIDs ranging from 50 μm diameter down to 200 nm at many locations on the chip allowing multi-terminal connections, or freeing some of the leads to be connected to other active component such as nanomechanical and micromechanical resonators.

Prior to the patterning of the junctions or SQUID loops we deposit a 50 nm thick pad of tungsten, (derived from the standard $W(CO)_6$ FIB deposition chemistry) but using electron beam rather than ion beam (5 KeV, 0.4 nA of beam current). For most devices a region of 5 μm square is sufficient but of course can be scaled accordingly. This protective layer allows us time to carefully align the ion beam with the device region so that patterning commences in the correct location and prevents undesirable ion exposure of the Nb film. Our typical target dimension for forming narrow nanobridges, which act as Josephson junctions, linking the SQUID loop is less than 60 nm wide. This is clearly incapable of being fabricated by optical lithography but is relatively simple for FIB. Typically using a 50 pA ion beam and x-y step size of 7 nm, with a 1 ms beam dwell time, running from our NPGS CAD drawing we will produce a nanoSQUID with each repeat of the pattern removing roughly 1 nm of Nb. Figure 8 shows two examples of Nb SQUIDs, with Figure 8a showing a 40 μm SQUID loop with FIB milled junctions and Figure 8b showing a 1 μm x 100 nm slot shaped nanoSQUID all milled by FIB. The electron beam deposited tungsten (lighter shade) is just visible around the ion-milled junctions in Figure 8a. These examples are just two of the geometries we currently work with.

4 Examples of Device Performance and Experiments

Turning now to the performance of our SQUID devices, Figure 9 shows a typical superconducting transition of a nanoSQUID device and the Nb film, with bias current of 180 μA. As can be seen there is a sharp transition at approximately 8.7 K corresponding to the T_c of the film with a drop to near, but not zero resistance. At this point our FIB fabricated junctions have not undergone a transition and are contributing the remaining resistance in the device. Lowering the temperature further results in a second, but less sharp, drop in resistance as the junctions themselves undergo a superconducting transition between 7.7 K and 7.5 K. The reason for the noisier transition here is that we have two junctions acting in parallel with very subtle differences in their behaviour. We believe, although have not proven that these differences are due to the fact that the grain size of our films is approximately the same size as an individual junction. This means that a single junction could be composed of one grain, or two with a grain boundary, or in very rare cases even a triple point.

Figure 10 shows a measurement of the bias current swept from zero to maximum current and back to zero for both positive and negative current directions, for a range of temperatures, indicating no hysteresis. Note that the shape of the plot is qualitatively similar to the classical

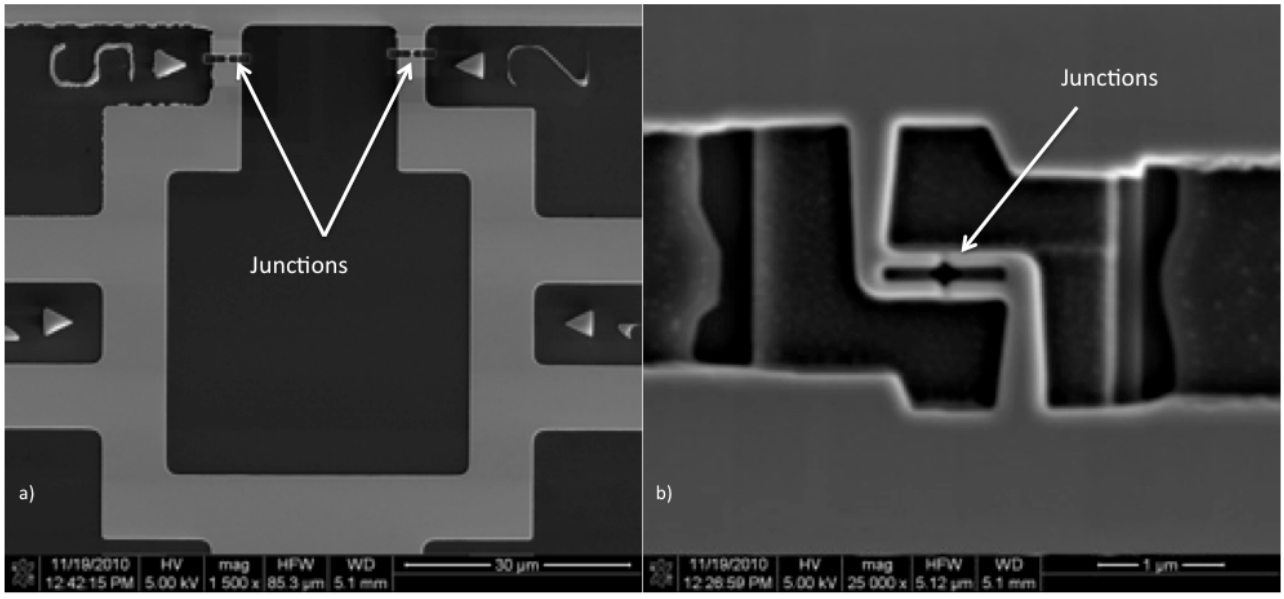

Figure 8: Two examples of a) FIB fabricated junctions, and b) a nanoSQUID loop.

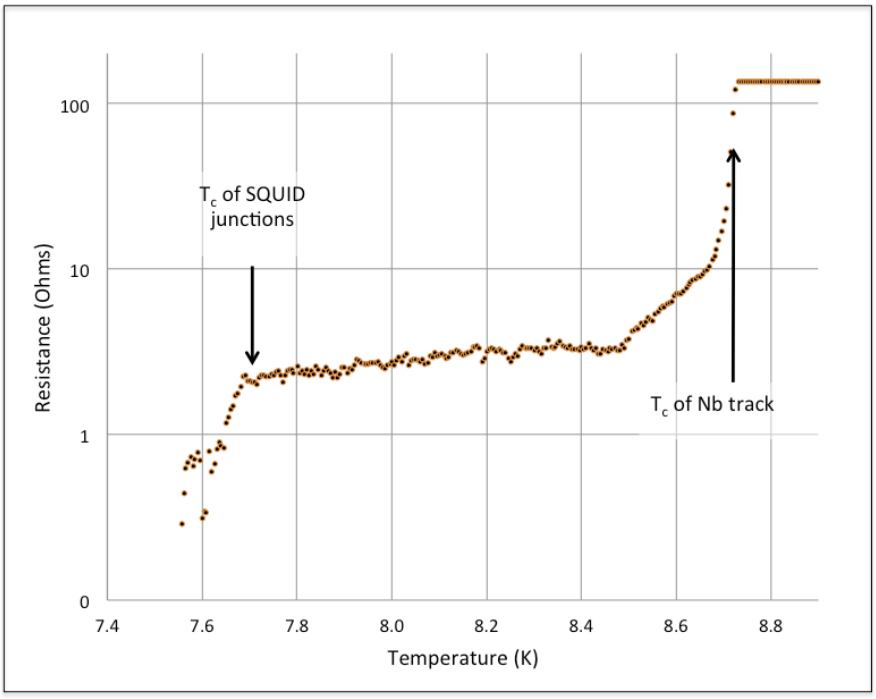

Figure 9: Superconducting transitions in Nb film and FIB fabricated junctions.

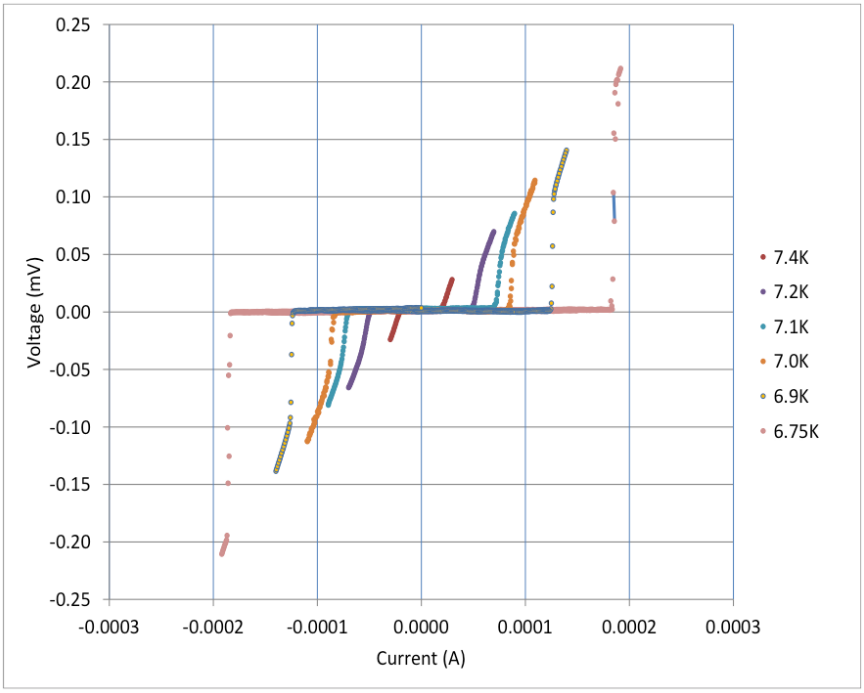

Figure 10: Current-voltage characteristic of a Nb nanoSQUID at a range of temperatures from T = 7.4 K to T = 6.75 K.

picture expected for a shunted Josephson junction, as described by the RSJ model. A zero voltage region is followed by a parabolic dependence of voltage on *dI*, the difference between the bias current and the critical current. The differential resistance for this device reached a value of about 1.2 Ohms in the usual operating region. In our SQUID devices the shunt resistance typically varies from 1 to 6 Ohms depending on the W deposition thickness and area on top of the Nb film.

The one aspect of our FIB fabricated nanoSQUIDs that is most outstanding is the noise performance of the devices. In Figure 11, the measured magnetic flux noise

spectral density $S\varphi$ expressed in units of the flux quantum $\phi 0/Hz^{1/2}$, as a function of frequency from 0.1 Hz to 100 kHz is shown. Note that there is a region at low frequency where the noise spectrum has a $1/f^2$ form, but above 1 Hz, there is a much weaker frequency dependence. Even at 1 Hz, the spectral density is as low as 0.8 $m\phi_0/Hz^{1/2}$, while in the white noise region around 1 kHz, this has fallen to 0.2 $m\phi_0/Hz^{1/2}$. The frequency roll off at higher frequencies represents the result of filtering in the readout electronics. A more complete description of measurement and noise performance of FIB milled Nb nanoSQUIDs is given in [15].

In addition to the advanced patterning capability of our FIB instrument we also make regular use of a nanomanipulation system. We have a four-probe Zyvex system with three-axis motion up to a range of 7 mm in each direction, and with step sizes as small as 20 nm. An example of an experiment involving FIB fabricated nanoSQUIDs and use of the manipulation system is shown in Figure 12. In this experiment we are investigating the use of a nanoSQUID to measure the presence of a single magnetic nanobead [19]. The four panels of Figure 12 show from the top left, a distribution of magnetic nanoparticles on a Si substrate, and approaching the substrate is a single FIB sharpened 7 μm diameter carbon fibre acting as

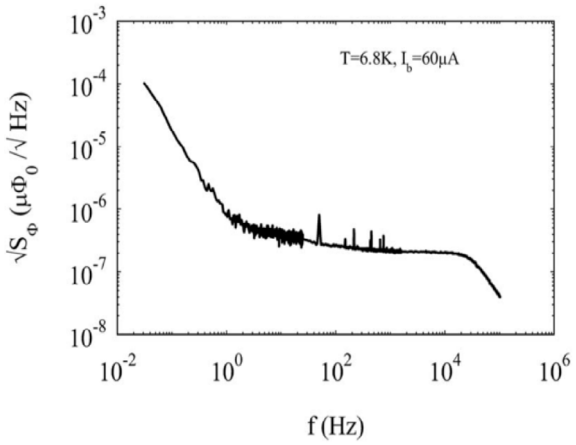

Figure 11: Flux noise spectral density versus frequency for a Nb nanoSQUID loop (350 nm diameter) at T = 6.8 K in zero magnetic field.

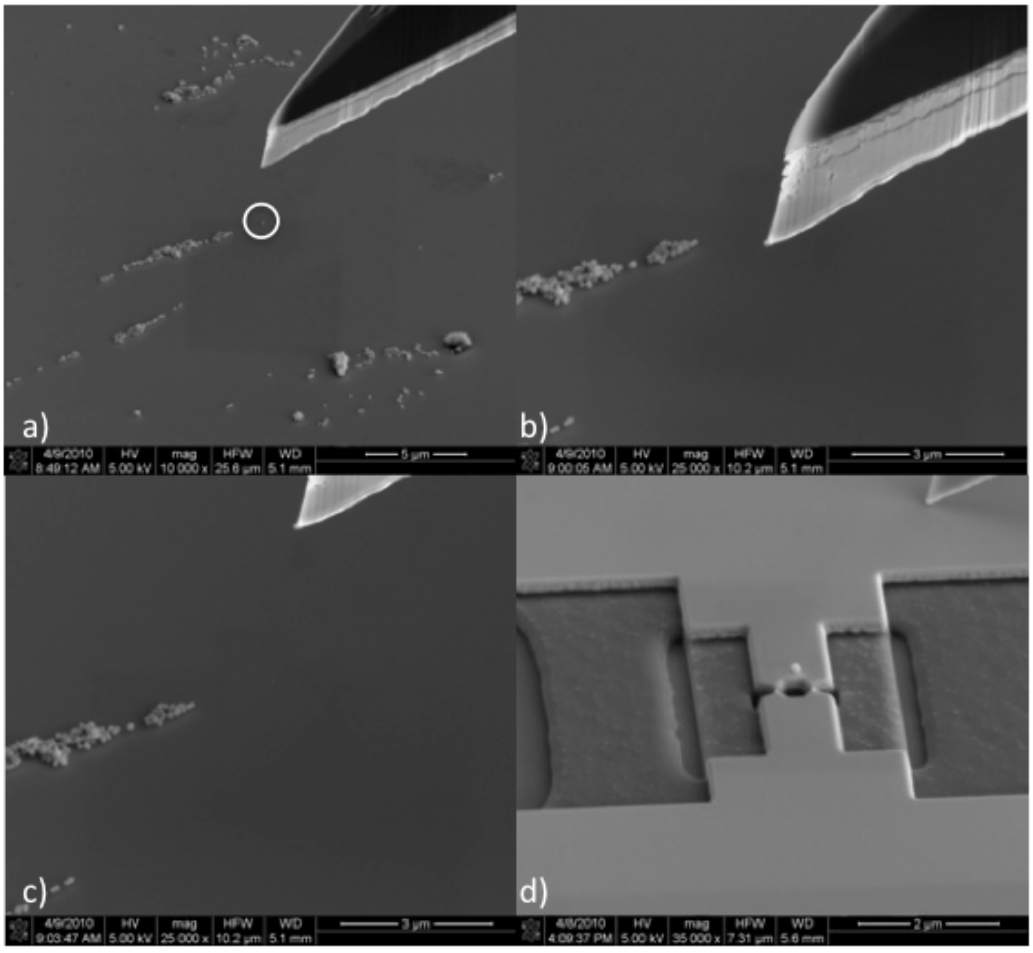

Figure 12: Manipulation of a single magnetic bead and its location on a nanoSQUID. a) Moving the sharpened tip into close proximity, target bead is shown inside the white ring. b) Lifting the bead from the surface. c) Moving the bead clear of the surface to the SQUID chip. d) Placing the bead on the 350 nm diameter nanoSQUID.

our manipulation tip. The particles are 60:40 Pt:Fe alloy with a range of diameter of 70 nm to 200 nm. The top right panel shows the tip just lifting a single particle (<150 nm diameter) from the Si with the lower left panel showing the tip moving away from substrate with particle clearly attached. Finally the lower right panel shows the particle in place on the edge of the SQUID loop.

Figures 13a and 13b show the response we see from the nanoSQUID with and without the bead when we sweep an external magnetic field applied in parallel to the SQUID loop. Figure 13a shows the response of the SQUID when no bead is present and as can be seen almost no hysteresis is present comparing the up and down sweep of the field. In Figure 13b the SQUID shows a strong and clear hysteretic response when the bead is present. Here the y-axis is showing the output from the SQUID amplifier we use in this experiment. More details of this experiment can be found in [19].

Figure 14 shows the hysteretic SQUID response to variation in magnetic field when the bead is present. As can be seen the SQUID easily detects the bead in a field of 10 mT and can be seen as low as 3 mT. Results such as this point to FIB fabricated nanoSQUIDs being ideal candidates for use in scanning SQUID microscopes. As we only need simple fabrication methods it is quite possible that a nanoSQUID could be fabricated on an AFM cantilever and the excellent response and low noise of the nanoSQUID could be used to map the local magnetic field of a sample with high spatial and field resolution.

Analysing the sensitivity of a range of sizes of our FIB fabricated nanoSQUIDs with a range of different magnetic particles shows that the spin sensitivity of the devices scales with the loop sizes. Extrapolation of the performance suggests that the ultimate limit of our 350 nm nanoSQUIDs might be as low as 2 spins/$Hz^{1/2}$ (Figure 15) but so far we have not carried out such an experiment. That our sensitivity is still a significant margin above both the thermal limit at the operating temperature and the quantum limit suggests with suitable care we may in fact be able to detect single spins with these devices. Furthermore, another very recent study has shown Nb nanoSQUID loops operating with weak link junctions and fabricated on the end of SNOM (scanning near field optical microscope) tips [20]. These devices have even lower flux noise performance than our own devices and should achieve single spin detection. These nanoSQUIDs are however considerably more complex to fabricate, and likely to offer lower yield than our simple FIB fabricated devices, but it further demonstrates that nanoSQUIDs offer a route to single spin detection.

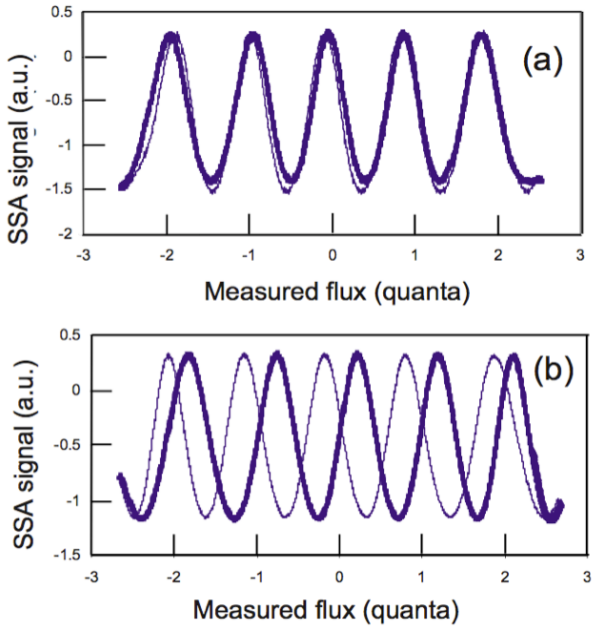

Figure 13: (a) SQUID output at 7.8 K with no particle present (the thin line is field sweep up, thick line is field sweep down) (b) SQUID output with a single FePt nanobead present at same temperature showing hysteresis.

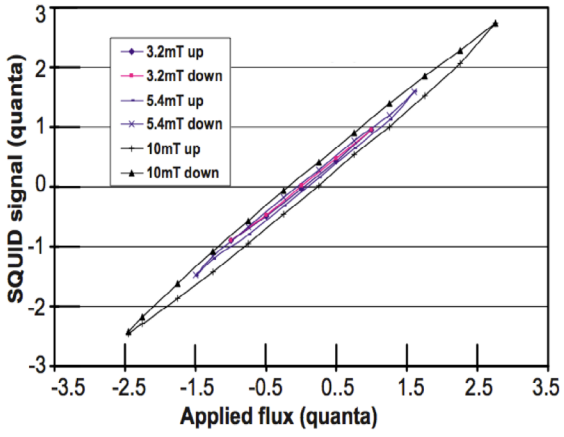

Figure 14: Hysteresis plots for the single FePt nanobead for a range of applied magnetic fields.

Using nanomanipulation allows us to insert structures other than small magnetic particles into our SQUID devices. The combination of a SQUID and nanomechanical resonator at the nanoscale will achieve novel states of coupled systems, such as the quantum mechanical ground state of a mechanical oscillator. Consequently we are developing novel fabrication techniques which allow integration of NEMs resonators with ultra-low noise nanoSQUIDs where the nanoSQUID senses the displacement of a NEMS resonator by inductively coupling a conducting mechanical resonator

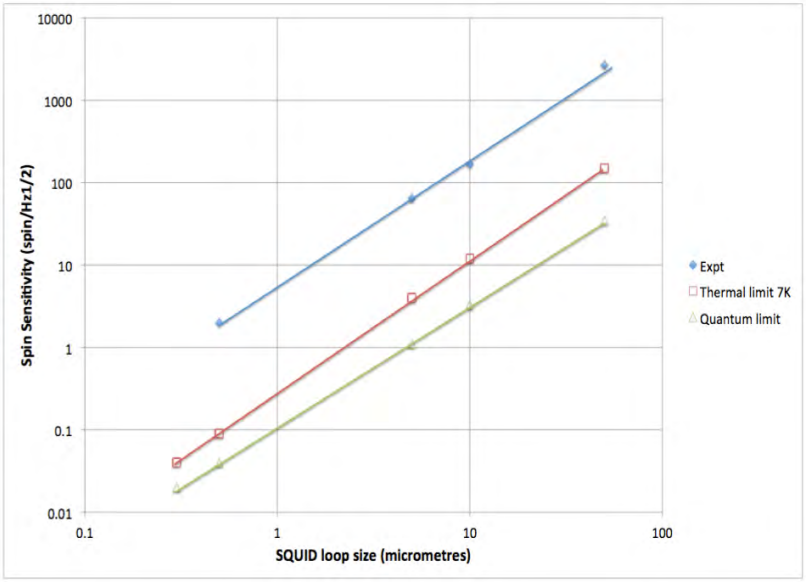

Figure 15: Spin sensitivity of FIB fabricated SQUID devices.

to the SQUID loop, where the shape and dimensions of the two elements should be as nearly matched as possible and the two should be brought into close contact [21]. Using FIB different SQUID loop structures can be made to match the mechanical resonators to optimize the filling factor. The calculated resonant frequencies of such a beam are in the range from 10 to 100 MHz, conveniently within the operating range of nanoSQUIDs.

5 Discussion and Summary

Using a very simple method we have developed a range of Nb based SQUID devices. The combination of very basic optical lithography and FIB allows us to produce SQUID loops on a sub-micron scale with a very high consistency of performance from device to device, but at the same time gives us the option to make every device unique should we choose. This fabrication method results in some of the most sensitive and low noise devices ever fabricated and may offer a route to the measure of single spins. The key to our device performance is based on the fact that during ion milling we produce a parallel shunt resistor that protects the device junctions when superconductivity breaks down. In turn, creating the device junctions with shunts means we do not have to attempt to make the junctions as small as is possible. Indeed, if we were to do this, the devices would not function as the junctions would not be superconducting.

We are still developing a better understanding of the role of the 'real' superconducting junction size that is produced by ion milling. We have however found that by further Ga ion dosing of the junctions we have a degree of control of their T_c. Our devices have a tendency to operate only one or two K below the superconducting transition of the film. We have found that once a device is fabricated and the T_c of the junctions is established, we can use the FIB to further dose the junctions, where we use low beam currents and at most a few hundred passes of the beam. This process of course removes small amounts of Nb but also moves the implanted and damaged front further into the junction. What this does in effect is reduce the size of the superconducting Nb grains in the junction region. It has been shown in both [22] and [23] that the superconducting transition in nanostructured Nb films can be lowered by reducing the grain size of the material. A monotonic reduction in T_c is observed with reducing grain size once it is smaller than approximately 28 nm, with the superconducting transition completely eliminated once the grain size is smaller than 8 nm. Based on the measured size of our junctions and knowledge of the implant depth for a 30 keV Ga ion we estimate our junctions are exactly of the dimensions to place them in the region where T_c is reduced. This simple mechanism is the underlying reason that enables our weak link junctions to function. We can, within reason, lower the T_c by repeated doses in increments as low as 0.1 K, but it must be born in mind that the inherent small variation in the number of grains in the junction region makes this at present a slightly imprecise method. We are however using this method to tune the T_c of Nb films in SQUID bolometers, for single photon and ion detection, where we have a need for an

absorber region in a SQUID loop with a T_c lower than the junction regions that in turn require a lower T_c than the films on which they are based [24].

As well as improving our understanding of interesting basic physics the production of superconducting devices by FIB lends itself well to rapid prototyping of devices in experiments where measurements using SQUIDs have a natural affinity. The measurement capabilities of SQUIDs are very diverse and cover a huge range of areas such as magnetic, electrical, thermal and mechanical measurements. In addition, and of great importance for the National Physical Laboratory, there has been little metrological activity to anticipate the impending metrological needs which exploitation of nanoSQUIDs and other nanoscale systems will require.

Acknowledgments: This work was funded by the UK NMS Program and the EU EMRP Project MetNEMS (NEW-08). The EMRP is jointly funded by EMRP participating countries within EURAMET and the European Union.

References

[1] Clarke J., Braginski A., ed., The SQUID Handbook Fundamentals and Technology of SQUIDs and SQUID Systems, 2004, 1, New York: Wiley–VCH.

[2] Koelle D., Kleiner R., Ludwig F., Danster E., Clarke J., High-transition-temperature superconducting quantum interference devices, Rev. Mod. Phys., 1999, 71 631; Erratum, Rev. Mod. Phys., 1999, 71, 1249.

[3] Gallop J.C., SQUIDs: some limits to measurement, Supercond. Sci. Technol., 2003, 16, 1575.

[4] Hilgenkamp H., Mannhart J., Grain boundaries in high-Tc superconductors, Rev. Mod. Phys., 2002, 74, 485.

[5] Veauvy C., Hasselbach K., Mailly D., Scanning μ-superconduction quantum interference device force microscope, Rev. Sci. Instrum., 2002, 73, 3825-3830.

[6] Hilgenkamp H., Ariando, Smilde H.J., Blank D., Rijnders G., Rogalla H., et al., Ordering and manipulation of the magnetic moments in large-scale superconducting pi-loop arrays, Nature, 2003, 422, 50-53.

[7] Hao L., Macfarlane J.C., Lam S.K.H., Foley C.P., Josephs-Franks P., Gallop J.C., Inductive Sensor Based on Nano-scale SQUIDs, IEEE Trans. Appl. Supercond., 2005, 15, 514-517.

[8] Awschalom D.D., Rozen J.R., Ketchen M.B., Gallagher W.J., Kleinsasser A.W., Sandstrom R.L., Bumble B., Low-noise modular microsusceptometer using nearly quantum limited dc SQUIDs, Appl. Phys. Lett., 1986, 53, 2108.

[9] Lam S.K.H., Tilbrook D.L., Development of a niobium nanosuperconducting quantum interference device for the detection of small spin populations, Appl. Phys. Lett., 2003, 82, 1078-1080.

[10] Cleuziou J.P., Wernsdorfer W., Bouchiat V., Ondarcuhu T., Nonthioux M., Carbon nanotube superconducting quantum interference device, Nat. Nanotechnol., 2006, 1, 53-59.

[11] Gallop J., Josephs-Franks P.W., Davis J., Hao L., Macfarlane J., Miniature dc SQUID devices for the detection of single atomic spin-flips, Physica C, 2002, 368, 109-113.

[12] Hao L., Gallop J.C., Cox D., Romans E., Macfarlane J.C., Chen J., Focused Ion Beam NanoSQUIDs as Novel NEMS Resonator Readouts, IEEE Trans. Appl. Supercond., 2009, l19, 693-696.

[13] Troeman A.G.P., Derking H., Borger B., Pleikies J., Veldhuis D., Hilgenkamp H., NanoSQUIDs Based on Niobium Constrictions, Nano Lett., 2007, 7, 2152-2156.

[14] Hao L., Macfarlane J.C., Gallop J.C., Romans E., Cox D., Hutson D., Chen J., Spatial resolution assessment of Nano-SQUIDs made by focused ion beam, IEEE Trans. Appl. Supercond., 2007, 17, 742-745.

[15] Hao L., Macfarlane J.C., Gallop J.C., Cox D., Beyer J., Drung D., Schurig T., Measurement and noise performance of nano-superconducting-quantum-interference devices fabricated by focused ion beam, Appl. Phys. Lett., 2008, 92, 192507.

[16] Calculated using SRIM (Stopping Range of Ions in Matter). www.srim.org.

[17] Additional calculations using SUPRE (Surrey University Sputter Profile Resolution and Energy deposition programme). www.surrey.ac.uk/ati/ibc/research/modelling_simulation/suspre.htm.

[18] Nanometer Pattern Generation System (NPGS). www.jcnabity.com.

[19] Hao L., Aßmann C., Gallop J.C., Cox D.C., Ruede F., Kazakova O., et al., Detection of Single Magnetic Nanobead with a Nano-Superconducting Quantum Interference Device, Appl. Phys. Lett., 2011, 98, 092504.

[20] Vasyukov D., Anahory Y., Embon L., Halbertal D., Cuppens J., Neeman L., et al., A scanning superconducting quantum interference device with single electron spin sensitivity, Nat. Nanotechnol., 2013, 8, 639-644.

[21] Hao L., Cox D.C., Gallop J.C., Chen J., Rozhko S., Blois A., Romans E.J., Coupled NanoSQUIDs and Nano-Electromechanical Systems (NEMS) Resonators, IEEE Trans. Appl. Supercond., 2013, 23, 1800304.

[22] Jin Y.R, Song X,H., Zhang D.L., Grain-size dependence of superconductivity in dc sputtered Nb films, Science in China Series G, Physics Mechanics & Astronomy, 2009, 52, 1289-1292.

[23] Bose S., Raychaudri P., Banerjee R., Vasa P., Ayyub P., Mechanism of the Size Dependence of the Superconducting Transition of Nanostructured Nb, Phys. Rev. Lett., 2005, 95, 147003.

[24] Work currently in progress.